HHS Public Access

Author manuscript

J Phys Chem Lett. Author manuscript; available in PMC 2018 July 06.

Published in final edited form as:

J Phys Chem Lett. 2017 July 06; 8(13): 3008–3014. doi:10.1021/acs.jpclett.7b00987.

Long-Lived $^{13}C_2$ Nuclear Spin States Hyperpolarized by Parahydrogen in Reversible Exchange at Micro-Tesla Fields

Zijian Zhou[1], **Jin Yu**[1], **Johannes F. P. Colell**[1], **Raul Laasner**[2], **Angus Logan**[1], **Danila Barskiy**[3], **Roman Schepin**[4], **Eduard Y. Chekmenev**[4], **Volker Blum**[1,2], **Warren S. Warren**[1,4], and **Thomas Theis**[1,*]

[1]Department of Chemistry, Duke University, Durham NC 27708, United States

[2]Department of Mechanical Engineering and Materials Science, Duke University, Durham NC 27708, United States

[3]Departments of Radiology, Biomedical Engineering and Physics, Vanderbilt University, Institute of Imaging Science (VUIIS), Nashville, TN 37232, United States

[4]Departments of Radiology, Physics and Biomedical Engineering, Duke University, Durham NC 27708, United States

Abstract

Parahydrogen is an inexpensive and readily available source of hyperpolarization used to enhance magnetic resonance signals by up to 4 orders of magnitude above thermal signals obtained at ~10 T. A significant challenge for applications is fast signal decay after hyperpolarization. Here, we use parahydrogen based polarization transfer catalysis at micro-Tesla fields (first introduced as SABRE-SHEATH) to hyperpolarize $^{13}C_2$ spin pairs and find decay time constants of 12 s for magnetization at 0.3 mT, which are extended to 2 minutes at that same field, when long-lived singlet states are hyperpolarized instead. Enhancements over thermal at 8.5 T are between 30 and 170 fold (0.02% to 0.12% polarization). We control the spin dynamics of polarization transfer by choice of μT field allowing for deliberate hyperpolarization of either magnetization or long-lived singlet states. Density functional theory (DFT) calculations and experimental evidence identify two energetically close mechanisms for polarization transfer: First, a model that involves direct binding of the $^{13}C_2$ pair to the polarization transfer catalyst (PTC), and second, a model transferring polarization through auxiliary protons in substrates.

Graphical Abstract

*Corresponding Author: To whom correspondence should be addressed. thomas.theis@duke.edu.

The authors declare no competing financial interests.

ASSOCIATED CONTENT

Supporting Information Details about substrate synthesis, experimental setup, and Matlab simulation (Spinach package) data are available online.

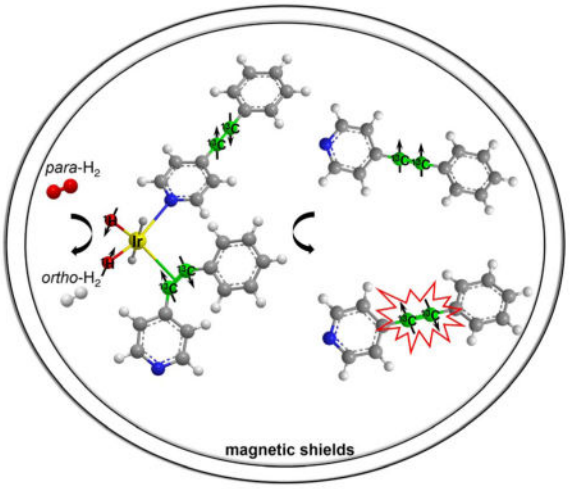

Nuclear spin hyperpolarization is an intriguing research area, because of its ability to enhance nuclear magnetic resonance (NMR) and magnetic resonance imaging (MRI) signals by multiple orders of magnitude.[1–5] Hyperpolarization methods are particularly useful if they can enhance signals from heteronuclei such as ^{13}C or ^{15}N because they can be installed in a wide range of biomolecules, and they retain hyperpolarization on extended timescales.[6–14] At the same time, hyperpolarization of protons also has particular advantages, which stem from higher sensitivity and 100% natural abundance. A particularly simple hyperpolarization technique is *para*-H_2 induced polarization (PHIP).[15–16] Especially, when implemented as Signal Amplification By Reversible Exchange (SABRE) it allows for continuous and rapid hyperpolarization directly in solutions.[17–18] In the SABRE procedure, *para*-H_2 and the target (*i.e.* to-be-hyperpolarized) molecules bind reversibly with an iridium-based hexacoordinate catalyst[19]. At specific magnetic fields, polarization will transfer from *para*-H_2 to spins on the target molecule driven by *J*-coupling interactions, for example ~6.5 mT is ideal to hyperpolarize proton spins.[17–18] On the other hand, heteronuclei (*e.g.* ^{15}N, ^{31}P, ^{13}C) are best magnetized in microTesla fields established in magnetically shielded environments, [20–22] an approach that was coined SABRE-SHEATH (SABRE in Shield Enable Alignment Transfer to Heteronuclei).

However, if the goal is to hyperpolarize long-lived singlet states,[6, 23–27] the picture changes slightly because the conditions for the transfer of scalar order have a different field dependence. For example, it has been shown that the singlet state of the $^{15}N_2$ spin pair of diazirines is hyperpolarized over a relatively wide range of magnetic fields between a few μT to about 100 mT.[28] These hyperpolarized nuclear spin singlet states of $^{15}N_2$ diazirines display relaxation time constants of above 20 minutes. Similarly, SABRE was used to hyperpolarize long-lived singlet states on $^{1}H_2$-pairs,[29–30] where polarization decay time constants of above 4 min were observed.[31] Such long hyperpolarization lifetime promises biomolecular tracking and imaging of low concentration analytes on significantly extended timescales. In this article, we use SABRE-SHEATH, to hyperpolarize magnetization as well as long-lived nuclear singlet states in carbon-13 spin pairs and find lifetime T_1 of 12 s for magnetization and T_S of 2 min for long-lived singlet states at 0.3 mT. Here it is important to

note, that the current record of a long-lived singlet state is held by a $^{13}C_2$ spin pair (hyperpolarized by DNP, not SABRE) with lifetime, T_S, of more than one hour.[6]

For the presented experiments, we designed two molecules with various isotopic labeling schemes. We synthesized 1,2-(4-pyridyl) acetylene, with symmetric structure, and 1-phenyl-2-(4-pyridyl) acetylene, with asymmetric structure. For both, we consider isotopomers with naturally abundant ^{13}C, as well as doubly ^{13}C labeled substrates at the triple bond. The results presented in Figure 1 indicate that the acetylene carbon spins as well as the aromatic bridge carbon spins are hyperpolarized. The enhancements are between 30 to 170 fold (0.02% to 0.12% polarization), when compared to thermal signals acquired at 8.45 T. The molecules with ^{13}C at natural abundance show 2–3 times higher enhancements compared to ^{13}C enriched sites. This is likely due to faster T_1 relaxation in $^{13}C_2$ pairs as opposed to T_1 of isolated ^{13}C spins. An additional cause may simply be the higher ratio of polarization source (p-H_2) to target spins in the naturally abundant case.[32]

The hyperpolarization transfer from *para*-H_2 to these substrates occurs via iridium based polarization transfer catalysts (PTC's). We used the standard precatalyst [IrCl(IMes)(COD)], (IMes = 1,3-bis(2,4,6-trimethylphenyl)imidazole-2-ylidene; COD = cyclooctadiene).[18–19] We used substrate concentrations of 30 mM or 160 mM, and catalyst concentrations of 2 mM or 10 mM for the symmetric and asymmetric compounds respectively. The solvent was methanol-d_4, and the pre-catalyst was activated by bubbling *para*-H_2 through the sample for 15 minutes at a pressure of 7 bar and a fractional parahydrogen enrichment of ~85%. Thereafter, hyperpolarization was performed according to the SABRE-SHEATH procedure:[10, 20, 28] the sample is exposed to *para*-H_2 in a magnetically shielded environment outfitted with a small solenoid coil to obtain a controllable μT magnetic field. One minute of exposure to *para*-H_2 is sufficient to equilibrate polarization. Subsequently, the sample is transferred manually as quickly as possible (~ 8 s) to a Bruker 360 MHz (8.45T) magnet for read out. The manual transfer time of 8 s is relatively consistent, with variations of ~1 s.

The polarization transfer occurs in catalytically active PTC's. Two possible, energetically low PTC species are depicted in Figure 2. The ground state energies were determined by density functional theory calculations using the all-electron FHI-aims code.[33] The geometries were optimized using the PBE parameterization of exchange and correlation[34] with a van der Waals correction[35] and the *tier 2* basis sets[33, 36]. Scalar relativity was handled in the atomic ZORA approximation. [33] Additional possible configurations and the corresponding PTC-energy landscape are provided in the Supplemental Information (SI). Furthermore, we provide ^1H-NMR spectra of the hyperpolarized hydrides bound to the Iridium center demonstrating the presence of at least two catalytic species. In this first study, we were not able to detect hyperpolarized ^{13}C signals from molecules bound to the Iridium molecules. Therefore, we rely on more indirect evidence coupled with ab initio calculations to determine likely PTC structures.

In the first PTC model (Figure 2A), all substrate molecules bind to the Ir center via nitrogen. This is the energetically lowest PTC species identified by us. Here, polarization transfers from *para*-H_2 to the pyridyl protons first and finally arrives at the acetylenic carbons. In the

second PTC model (Figure 2B), the catalyst binds with the triple bond and polarization is transferred directly to ^{13}C sites.

The spectra displayed in Figure 1 could quickly lead to the conclusion, that the active PTC must be the directly binding model (Figure 2B), because we do not observe hyperpolarization from the ring carbons, other than from those in the bridge to the acetylene bond. Moreover, we observe hydrogenation, which most certainly requires binding of the triple bond to the iridium center. Hydrogenation rates depend on the ratio of substrate to catalyst: at 3:1 hydrogenation completes in less than 30 minutes, however at above 15:1, hydrogenation takes more than 12 h. In a single SABRE experiment (with 1 min of bubbling) we estimate significantly less than 1% hydrogenation at the 15:1 ratio, which was used for most experiments. We even observe hyperpolarized hydrogenation products that display typical ALTADENA type enhancements due to incorporation of *para*-H_2 (spectra provided in the SI), still, keeping in mind that the displayed spectra of Fig. 1 must all result from SABRE as they are uniquely associated with the intact, non-hydrogenated substrates.

However, these conclusions may be premature. First, the PTC on of Figure 2A is energetically lower. Furthermore, notice that all non-detected ^{13}C spins are directly bound to protons. This leads to much faster ^{13}C relaxation (a typical T_1 relaxation time for aromatic ^{13}C directly bound to a proton is ~5s see Ref.[37], whereas T_1 relaxation constants of the bridge carbons are found to be 11(1) s and T_1 of the acetylenic carbons is 12(0.5) s at low fields) with two important consequences. First, the hyperpolarization buildup at these ^{13}C sites will be much less efficient, and second, a small amount of hyperpolarization may quickly relax during the ~8 s sample transfer from polarization region into the magnet. In addition, we performed SABRE under optimized condition for ^{1}H polarization transfer at 6.5 mT, and this resulted in strong enhancement of the pyridyl ring protons, while enhancement of ^{13}C were negligible and ^{1}H enhancements on the distant phenyl ring were much smaller. Though bound species are never observed from the ^{13}C spectra, the hydride peaks are available in the SI. We observe a small chemical shift difference of the hydride peaks (~0.2 ppm, which would be much larger for the binding mode in Figure 2B based on DFT calculation). Finally, we attempted to hyperpolarize diphenyl-$^{13}C_2$-acetylene (no ring nitrogens) in the SABRE-SHEATH mode and did not observe enhancements. All these considerations point to a strong contribution of the PTC shown in Figure 2A.

To investigate this in more detail, we performed a careful characterization of hyperpolarization transfer as function of micro-Tesla field using the doubly ^{13}C labeled molecules. As depicted in Figure 3, we varied the magnetic field between −12 and +12 μT, accompanied by simulations of the hyperpolarization transfer process.

The first important finding is that we can directly choose to polarize different states of the ^{13}C pair: magnetization or singlet, which are easily distinguishable by their spectra. Magnetization is easily detected from both molecules (Figure 3 A1, B1), whereas singlet-order can only be detected immediately from the asymmetric 1-phenyl-2-(4-pyridyl) acetylene because the acetylenic carbons have a chemical shift difference (Figure 1C). For this asymmetric compound, the acetylenic carbons are strongly coupled at low fields (J_{CC} is ~185 Hz, whereas their chemical shift difference $\Delta\nu_C$ is less than 0.5 mHz). Upon transfer

to the high field in the magnet (8.45 T) for read out, the chemical shift difference becomes significantly larger than the J_{CC} coupling ($\Delta\nu_C$ ~770 Hz), the carbons are now weakly coupled, and the singlet state is no longer an eigenstate. The sample transfer from low to high field transforms $\boldsymbol{I}_1 \cdot \boldsymbol{I}_2$ singlet order into detectable ($I_{1z} - I_{2z}$) which gives antiphase signals in a pulse acquire experiment, as shown in Figure 3 (B4) (Full analysis of singlet order transfer is provided in the SI). However, for the symmetric molecule, since the two carbons will remain symmetric at high field, the singlet state cannot be accessed immediately. In principle, access to the singlet can be accomplished by specialized pulse sequences such as singlet-to-magnetization (S2M)[38–39] or SLIC,[40–41] yet this is beyond the scope of the present work.

In order to understand the polarization transfer dynamics at micro-Tesla fields in detail, we consider resonance conditions dictated by the Hamiltonian of the doubly ^{13}C labeled molecule. As detailed in the SI, at low fields of <0.6 μT, we encounter a resonance condition to polarize magnetization, given as

$$|\nu_H - \nu_C| = \pm J_{\mathrm{HH}}, \quad \text{(Eq.1)}$$

where ν_H and ν_C are the frequencies of protons and carbons and J_{HH} is the *J*-coupling between the two *para*-H_2 derived hydrides on the iridium. When solved for the magnetic field using $\nu = -\gamma B$ we obtain the magnetization transfer field as

$$B_{\mathrm{trans}} = \pm J_{\mathrm{HH}}/(\gamma_H - \gamma_C), \quad \text{(Eq. 2)}$$

where γ_H=42.577 Hz/μT and γ_C=10.705 Hz/μT. When the field is increased to a few μT, additional resonance conditions to create magnetization and/or singlet are encountered. The Hamiltonian reveals overlapping conditions to create magnetization and singlet given as

$$|\nu_H - \nu_C| = \pm (J_{\mathrm{CC}} \pm J_{\mathrm{HH}}), \quad \text{(Eq. 3)}$$

where J_{CC} is the acetylenic ^{13}C *J*-coupling. Again, solving for the transfer field we obtain:

$$B_{\mathrm{trans}} = \pm (J_{\mathrm{CC}} \pm J_{\mathrm{HH}})/(\gamma_H - \gamma_C) \quad \text{(Eq. 4)}$$

Equations (1,2) and (3,4) fully encompass the behavior observed in Figure 3. In the low field region, maximum magnetization transfer is observed at ~ ± 0.34(0.1) μT, whereas there is negligible singlet buildup. At slightly elevated fields, both magnetization and singlet have local maxima/minima at ~ ±5.6(0.2) μT and ~ ±6.4(0.2) μT (see Fig. 3B). These values are consistent with J_{HH} ~ 10(3) Hz, and J_{CC} ~190(5) Hz. J_{CC} can also be estimated from the

hyperpolarized NMR spectrum of the free form where we find J_{CC} = 185 Hz (see Fig. 1 panel D).

By numerical simulations of the spin dynamics we confirm that the general behavior is largely independent of the polarization transfer mechanism (direct to $^{13}C_2$ (Fig. 2B) vs. indirect via auxiliary protons (Figure 2A); see SI for details). However, the numerical value of J_{CC} strongly depends on the exact nature of the PTC. We have performed first principles calculations of the relevant *J*-couplings using the FHI-aims code.[33] We used the PBE[34] parameterization for exchange and correlation and the fully uncontracted cc-Pv5Z[42] basis sets (*tier 2* for iridium[33]). The *ab initio* calculations predict a J_{CC} of ~191 Hz for substrate bound via nitrogen (Figure 2A) vs. a J_{CC} of 120 Hz for substrate bound directly via the acetylenic bond (see full details in the SI). Based on the measurements shown in Figure 3, we can now conclude with more confidence that the primary PTC is the energetically favored species shown in Figure 2A because for the PTC in 2B we would expect efficient hyperpolarization at significantly lower fields of 3.5±0.3 μT, which is not observed.

Finally, since the asymmetric molecule allows for easy read out of, both, singlet state and magnetization, we can measure their lifetimes T_S or T_1. As displayed in Figure 4, we measured T_S at 0.3 mT and 50 mT, and fit with exponential decay constants of 117(7) s and 69(4) s respectively. For comparison, we measured T_1 at the field where it has longer T_S (0.3 mT) and find that magnetization decays much more rapidly with exponential decay constant T_1 of 12(.5) s. The T_1 lifetime of the $^{13}C_2$ pair at 8.45T is measured as 8(0.4) s.

In conclusion, we demonstrated that, both magnetization and long-lived singlet order can be induced on $^{13}C_2$ using SABRE-SHEATH. Hyperpolarization lifetime is extended to ~2 minutes, or 10 times T_1. Furthermore, we describe direct hyperpolarization of long-lived singlet order by SABRE-SHEATH when the *J*-coupling in the targeted spin pair is much larger than the J_{HH} coupling between the hydrides. This is in contrast to the first demonstration, of heteronuclear ($^{15}N_2$) long-lived states hyperpolarized by SABRE, where J_{NN} and J_{HH} were comparable in size leading to a resonance condition that is matched at a broad range of fields,[28] raising the question if long-lived states could be hyperpolarized when J_{NN} or J_{CC} are much larger. Here we have shown that specific μT-fields work in that case. Hyperpolarization levels and enhancements remained relatively low in this first demonstration. A likely culprit are the quadrupolar ^{14}N nuclei, as we are finding that quadrupoles act as highly efficient polarization sinks at μT fields. Therefore, we could likely boost hyperpolarization by additional ^{15}N labeling of our substrates and other strategies detailed in the literature.[43–45] Finally, we have also assembled clear evidence for at least two potential PTC species that simultaneously exist in solution and we presented arguments that lead us to believe that polarization transfer is primarily mediated indirectly via protons in the substrates. Overall, the presented results illustrate an avenue towards simple and fast hyperpolarization of long-lived ^{13}C hyperpolarization with potential applications in biomolecular MRI or the observation of slower processes by hyperpolarized NMR. The presented advances can be translated to biomolecules already shown to be amenable to heteronuclear SABRE hyperpolarization including nicotinamide[20, 46], *in vivo* pH sensor imidazole[47], hypoxia sensor metronidazole[43] and others.[10, 48] While the current work was performed in methanol solutions, recent advances in heterogeneous[49–50] and water-

soluble[51–56] SABRE catalysis may lead to *in vivo* translation of the presented approach for fast hyperpolarization of long-lived ^{13}C molecular probes.

Supplementary Material

Refer to Web version on PubMed Central for supplementary material.

Acknowledgments

The authors gratefully acknowledge the NSF (CHE-1363008 and CHE-1416268), ACS-Petroleum Research Fund 55835-ND6, NIH 1R21EB018014, U01 CA202229, 1R21EB020323, P41 EB015897, DOD CDMRP W81XWH-15-1-0271 and W81XWH-12-1-0159/BC112431 and ExxonMobil Knowledge Build for financial support of this research.

References

1. Ardenkjær-Larsen JH, Fridlund B, Gram A, Hansson G, Hansson L, Lerche MH, Servin R, Thaning M, Golman K. Increase in signal-to-noise ratio of > 10,000 times in liquid-state NMR. Proc Natl Acad Sci USA. 2003; 100(18):10158–10163. [PubMed: 12930897]
2. Ardenkjaer-Larsen J-H, Boebinger GS, Comment A, Duckett S, Edison AS, Engelke F, Griesinger C, Griffin RG, Hilty C, Maeda H, Parigi G, Prisner T, Ravera E, van Bentum J, Vega S, Webb A, Luchinat C, Schwalbe H, Frydman L. Facing and Overcoming Sensitivity Challenges in Biomolecular NMR Spectroscopy. Angew Chem Int Ed. 2015; 54(32):9162–9185.
3. Walker TG, Happer W. Spin-exchange optical pumping of noble-gas nuclei. Rev Mod Phys. 1997; 69(2):629–642.
4. Zheng Y, Miller GW, Tobias WA, Cates GD. A method for imaging and spectroscopy using γ-rays and magnetic resonance. Nature. 2016; 537(7622):652–655. [PubMed: 27680938]
5. Nelson SJ, Kurhanewicz J, Vigneron DB, Larson PE, Harzstark AL, Ferrone M, van Criekinge M, Chang JW, Bok R, Park I, Reed G, Carvajal L, Small EJ, Munster P, Weinberg VK, Ardenkjaer-Larsen JH, Chen AP, Hurd RE, Odegardstuen LI, Robb FJ, Tropp J, Murray JA. Metabolic imaging of patients with prostate cancer using hyperpolarized [1-(1)(3)C]pyruvate. Sci Transl Med. 2013; 5(198):198ra108.
6. Stevanato G, Hill-Cousins JT, Håkansson P, Roy SS, Brown LJ, Brown RCD, Pileio G, Levitt MH. A Nuclear Singlet Lifetime of More than One Hour in Room-Temperature Solution. Angew Chem Int Ed. 2015; 54(12):3740–3743.
7. Keshari KR, Wilson DM. Chemistry and biochemistry of 13C hyperpolarized magnetic resonance using dynamic nuclear polarization. Chem Soc Rev. 2014; 43(5):1627–59. [PubMed: 24363044]
8. Tee SS, DiGialleonardo V, Eskandari R, Jeong S, Granlund KL, Miloushev V, Poot AJ, Truong S, Alvarez JA, Aldeborgh HN, Keshari KR. Sampling Hyperpolarized Molecules Utilizing a 1 Tesla Permanent Magnetic Field. Sci Rep. 2016; 6:32846. [PubMed: 27597137]
9. Nonaka H, Hirano M, Imakura Y, Takakusagi Y, Ichikawa K, Sando S. Design of a 15N Molecular Unit to Achieve Long Retention of Hyperpolarized Spin State. Sci Rep. 2017; 7:40104. [PubMed: 28067292]
10. Colell JFP, Logan AWJ, Zhou Z, Shchepin RV, Barskiy DA, Ortiz GX, Wang Q, Malcolmson SJ, Chekmenev EY, Warren WS, Theis T. Generalizing, Extending, and Maximizing Nitrogen-15 Hyperpolarization Induced by Parahydrogen in Reversible Exchange. J Phys Chem C. 2017; 121(12):6626–6634.
11. Nikolaou P, Goodson BM, Chekmenev EY. NMR Hyperpolarization Techniques for Biomedicine. Chem Eur J. 2015; 21(8):3156–3166. [PubMed: 25470566]
12. Kurhanewicz J, Vigneron DB, Brindle K, Chekmenev EY, Comment A, Cunningham CH, Deberardinis RJ, Green GG, Leach MO, Rajan SS, Rizi RR, Ross BD, Warren WS, Malloy CR. Analysis of cancer metabolism by imaging hyperpolarized nuclei: prospects for translation to clinical research. Neoplasia. 2011; 13(2):81–97. [PubMed: 21403835]

13. Brindle KM. Imaging Metabolism with Hyperpolarized 13C-Labeled Cell Substrates. J Am Chem Soc. 2015; 137(20):6418–6427. [PubMed: 25950268]
14. Comment A, Merritt ME. Hyperpolarized Magnetic Resonance as a Sensitive Detector of Metabolic Function. Biochemistry-Us. 2014; 53(47):7333–7357.
15. Bowers CR, Weitekamp DP. Transformation of Symmetrization Order to Nuclear-Spin Magnetization by Chemical-Reaction and Nuclear-Magnetic-Resonance. Phys Rev Lett. 1986; 57(21):2645–2648. [PubMed: 10033824]
16. Eisenschmid TC, Kirss RU, Deutsch PP, Hommeltoft SI, Eisenberg R, Bargon J, Lawler RG, Balch AL. Para Hydrogen Induced Polarization in Hydrogenation Reactions. J Am Chem Soc. 1987; 109(26):8089–8091.
17. Adams RW, Aguilar JA, Atkinson KD, Cowley MJ, Elliott PI, Duckett SB, Green GG, Khazal IG, Lopez-Serrano J, Williamson DC. Reversible interactions with para-hydrogen enhance NMR sensitivity by polarization transfer. Science. 2009; 323(5922):1708–11. [PubMed: 19325111]
18. Cowley MJ, Adams RW, Atkinson KD, Cockett MCR, Duckett SB, Green GGR, Lohman JAB, Kerssebaum R, Kilgour D, Mewis RE. Iridium N-Heterocyclic Carbene Complexes as Efficient Catalysts for Magnetization Transfer from para-Hydrogen. J Am Chem Soc. 2011; 133(16):6134–6137. [PubMed: 21469642]
19. Vazquez-Serrano LD, Owens BT, Buriak JM. The search for new hydrogenation catalyst motifs based on N-heterocyclic carbene ligands. Inorg Chim Acta. 2006; 359(9):2786–2797.
20. Theis T, Truong ML, Coffey AM, Shchepin RV, Waddell KW, Shi F, Goodson BM, Warren WS, Chekmenev EY. Microtesla SABRE Enables 10% Nitrogen-15 Nuclear Spin Polarization. J Am Chem Soc. 2015; 137(4):1404–1407. [PubMed: 25583142]
21. Truong ML, Theis T, Coffey AM, Shchepin RV, Waddell KW, Shi F, Goodson BM, Warren WS, Chekmenev EY. 15N Hyperpolarization by Reversible Exchange Using SABRE-SHEATH. J Phys Chem C. 2015; 119(16):8786–8797.
22. Zhivonitko VV, Skovpin IV, Koptyug IV. Strong 31P nuclear spin hyperpolarization produced via reversible chemical interaction with parahydrogen. Chem Commun. 2015; 51(13):2506–2509.
23. Carravetta M, Johannessen OG, Levitt MH. Beyond the T1 limit: Singlet nuclear spin states in low magnetic fields. Phys Rev Lett. 2004; 92:153003. [PubMed: 15169282]
24. Carravetta M, Levitt MH. Long-lived nuclear spin states in high-field solution NMR. J Am Chem Soc. 2004; 126(20):6228–6229. [PubMed: 15149209]
25. Levitt MH. Singlet Nuclear Magnetic Resonance. Ann Rev Phys Chem. 2012; 63:89–105. [PubMed: 22224703]
26. Warren WS, Jenista E, Branca RT, Chen X. Increasing Hyperpolarized Spin Lifetimes Through True Singlet Eigenstates. Science. 2009; 323(5922):1711–1714. [PubMed: 19325112]
27. Vasos PR, Comment A, Sarkar R, Ahuja P, Jannin S, Ansermet JP, Konter JA, Hautle P, van den Brandt B, Bodenhausen G. Long-lived states to sustain hyperpolarized magnetization. Proc Natl Acad Sci U S A. 2009; 106(44):18469–18473. [PubMed: 19841270]
28. Theis T, Ortiz GX, Logan AWJ, Claytor KE, Feng Y, Huhn WP, Blum V, Malcolmson SJ, Chekmenev EY, Wang Q, Warren WS. Direct and cost-efficient hyperpolarization of long-lived nuclear spin states on universal 15N2-diazirine molecular tags. Sci Adv. 2016; 2(3):e1501438. [PubMed: 27051867]
29. Roy SS, Rayner PJ, Norcott P, Green GG, Duckett SB. Long-lived states to sustain SABRE hyperpolarised magnetisation. Phys Chem Chem Phys. 2016; 18(36):24905–24911. [PubMed: 27711398]
30. Olaru AM, Roy SS, Lloyd LS, Coombes S, Green GGR, Duckett SB. Creating a hyperpolarised pseudo singlet state through polarisation transfer from parahydrogen under SABRE. Chem Commun. 2016; 52(50):7842–7845.
31. Roy SS, Norcott P, Rayner PJ, Green GGR, Duckett SB. A Hyperpolarizable 1H Magnetic Resonance Probe for Signal Detection 15 Minutes after Spin Polarization Storage. Angew Chem Int Ed. 2016; 128(50):15871–15874.
32. Shchepin RV, Truong ML, Theis T, Coffey AM, Shi F, Waddell KW, Warren WS, Goodson BM, Chekmenev EY. Hyperpolarization of “Neat” Liquids by NMR Signal Amplification by Reversible Exchange. J Chem Phys Lett. 2015; 6(10):1961–1967.

33. Blum V, Gehrke R, Hanke F, Havu P, Havu V, Ren X, Reuter K, Scheffler M. Ab initio molecular simulations with numeric atom-centered orbitals. Comput Phys Commun. 2009; 180(11):2175–2196.
34. Perdew JP, Burke K, Ernzerhof M. Generalized Gradient Approximation Made Simple. Phys Rev Lett. 1996; 77(18):3865–3868. [PubMed: 10062328]
35. Tkatchenko A, Scheffler M. Accurate Molecular Van Der Waals Interactions from Ground-State Electron Density and Free-Atom Reference Data. Phys Rev Lett. 2009; 102(7):073005. [PubMed: 19257665]
36. Jensen SR, Saha S, Flores-Livas JA, Huhn W, Blum V, Goedecker S, Frediani L. The Elephant in the Room of Density Functional Theory Calculations. J Phys Chem Lett. 2017; 8(7):1449–1457. [PubMed: 28291362]
37. Barskiy DA, Shchepin RV, Tanner CPN, Colell JFP, Goodson BM, Theis T, Warren WS, Chekmenev EY. The Absence of Quadrupolar Nuclei Facilitates Efficient 13C Hyperpolarization via Reversible Exchange with Parahydrogen. Chemphyschem. 2017; doi: 10.1002/cphc.201700416
38. Tayler MCD, Levitt MH. Singlet nuclear magnetic resonance of nearly-equivalent spins. Phys Chem Chem Phys. 2011; 13(13):5556–5560. [PubMed: 21318206]
39. Feng Y, Theis T, Liang X, Wang Q, Zhou P, Warren WS. Storage of hydrogen spin polarization in long-lived 13C2 singlet order and implications for hyperpolarized magnetic resonance imaging. J Am Chem Soc. 2013; 135(26):9632–5. [PubMed: 23781874]
40. Devience, S., Walsworth, R., Rosen, M. Spin-locking induced crossing: J-coupling spectroscopy at high and low fields. Experimental NMR Conference; Pacific Grove, CA, Pacific Grove, CA. 2013.
41. Theis T, Feng Y, Wu T, Warren WS. Composite and shaped pulses for efficient and robust pumping of disconnected eigenstates in magnetic resonance. J Chem Phys. 2014; 140(1)
42. THD. Gaussian basis sets for use in correlated molecular calculations. I. The atoms boron through neon and hydrogen. J Chem Phys. 1989; 90(2):1007–1023.
43. Barskiy DA, Shchepin RV, Coffey AM, Theis T, Warren WS, Goodson BM, Chekmenev EY. Over 20%15N Hyperpolarization in Under One Minute for Metronidazole, an Antibiotic and Hypoxia Probe. J Am Chem Soc. 2016; 138(26):8080–8083. [PubMed: 27321159]
44. Rayner PJ, Burns MJ, Olaru AM, Norcott P, Fekete M, Green GGR, Highton LAR, Mewis RE, Duckett SB. Delivering strong 1H nuclear hyperpolarization levels and long magnetic lifetimes through signal amplification by reversible exchange. Proc Natl Acad Sci (USA). 2017; 114(16):E3188–E3194. [PubMed: 28377523]
45. Eshuis N, Hermkens N, van Weerdenburg BJA, Feiters MC, Rutjes FPJT, Wijmenga SS, Tessari M. Toward Nanomolar Detection by NMR Through SABRE Hyperpolarization. J Am Chem Soc. 2014; 136(7):2695–2698. [PubMed: 24475903]
46. Shchepin RV, Barskiy DA, Mikhaylov DM, Chekmenev EY. Efficient Synthesis of Nicotinamide-1–15N for Ultrafast NMR Hyperpolarization Using Parahydrogen. Bioconjug Chem. 2016; 27(4):878–882. [PubMed: 26999571]
47. Shchepin RV, Barskiy DA, Coffey AM, Theis T, Shi F, Warren WS, Goodson BM, Chekmenev EY. 15N Hyperpolarization of Imidazole-15N2 for Magnetic Resonance pH Sensing Via SABRE-SHEATH. ACS Sens. 2016
48. Logan AW, Theis T, Colell JF, Warren WS, Malcolmson SJ. Hyperpolarization of Nitrogen-15 Schiff Bases by Reversible Exchange Catalysis with para-Hydrogen. Chem Eur J. 2016; 22(31): 10777–81. [PubMed: 27218241]
49. Shi F, Coffey AM, Waddell KW, Chekmenev EY, Goodson BM. Nanoscale Catalysts for NMR Signal Enhancement by Reversible Exchange. J Phys Chem C. 2015; 119(13):7525–7533.
50. Shi F, Coffey AM, Waddell KW, Chekmenev EY, Goodson BM. Heterogeneous Solution NMR Signal Amplification by Reversible Exchange. Angew Chem Int Ed. 2014; 53(29):7495–7498.
51. Spannring P, Reile I, Emondts M, Schleker PPM, Hermkens NKJ, van der Zwaluw NGJ, van Weerdenburg BJA, Tinnemans P, Tessari M, Blümich B, Rutjes FPJT, Feiters MC. A New Ir-NHC Catalyst for Signal Amplification by Reversible Exchange in D2O. Chem Eur J. 2016; 22(27): 9277–9282. [PubMed: 27258850]

52. Shi F, He P, Best Q, Groome KA, Truong ML, Coffey AM, Zimay G, Shchepin RV, Waddell KW, Chekmenev EY, Goodson BM. Aqueous NMR Signal Enhancement by Reversible Exchange in a Single Step Using Water-Soluble Catalysts. J Phys Chem C. 2016; 120(22):12149–12156.

53. Hövener J-B, Schwaderlapp N, Borowiak R, Lickert T, Duckett SB, Mewis RE, Adams RW, Burns MJ, Highton LAR, Green GGR, Olaru A, Hennig J, von Elverfeldt D. Toward Biocompatible Nuclear Hyperpolarization Using Signal Amplification by Reversible Exchange: Quantitative in Situ Spectroscopy and High-Field Imaging. Anal Chem. 2014; 86(3):1767–1774. [PubMed: 24397559]

54. Rovedo P, Knecht S, Baumlisberger T, Cremer AL, Duckett SB, Mewis RE, Green GG, Burns M, Rayner PJ, Leibfritz D, Korvink JG, Hennig J, Putz G, von Elverfeldt D, Hovener JB. Molecular MRI in the Earth's Magnetic Field Using Continuous Hyperpolarization of a Biomolecule in Water. J Phys Chem B. 2016; 120(25):5670–7. [PubMed: 27228166]

55. Zeng H, Xu J, McMahon MT, Lohman JAB, van Zijl PCM. Achieving 1% NMR polarization in water in less than 1 min using SABRE. J Magn Reson. 2014; 246:119–121. [PubMed: 25123540]

56. Truong ML, Shi F, He P, Yuan B, Plunkett KN, Coffey AM, Shchepin RV, Barskiy DA, Kovtunov KV, Koptyug IV, Waddell KW, Goodson BM, Chekmenev EY. Irreversible Catalyst Activation Enables Hyperpolarization and Water Solubility for NMR Signal Amplification by Reversible Exchange. J Phys Chem B. 2014; 118(48):13882–13889. [PubMed: 25372972]

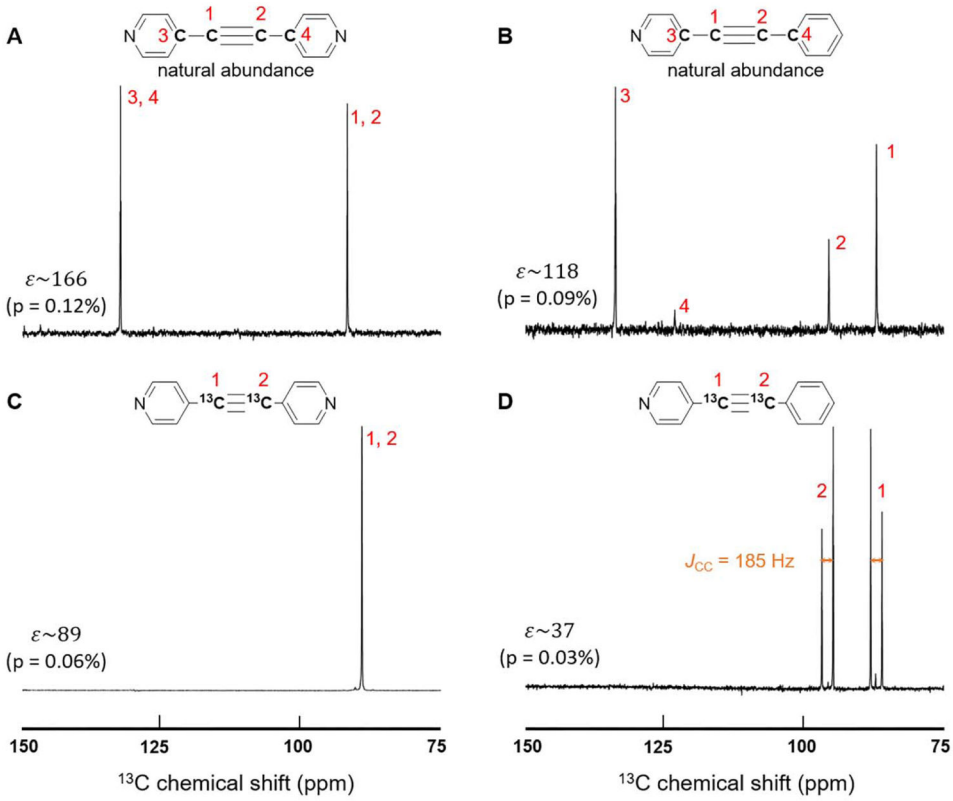

Figure 1.

^{13}C spectra of naturally abundant (A&B) and ^{13}C labelled (C&D) substrates used in experiments. A&C show results for the symmetrically substituted 1,2-2 pyridyl acetylene. B&D are from the asymmetrically substituted 1-phenyl-2-(4-pyridyl) acetylene. For the naturally abundant substrates the bridge carbons on the pyridyl rings (3, 4 in A, 3 in B) show significant enhancement, while the one on the benzene ring (4 in B) is only slightly hyperpolarized. The ^{13}C-^{13}C coupling, J_{CC}, read from the line-splitting in panel D is 185 Hz. (The SI also provides a thermal spectrum in Fig. S2.)

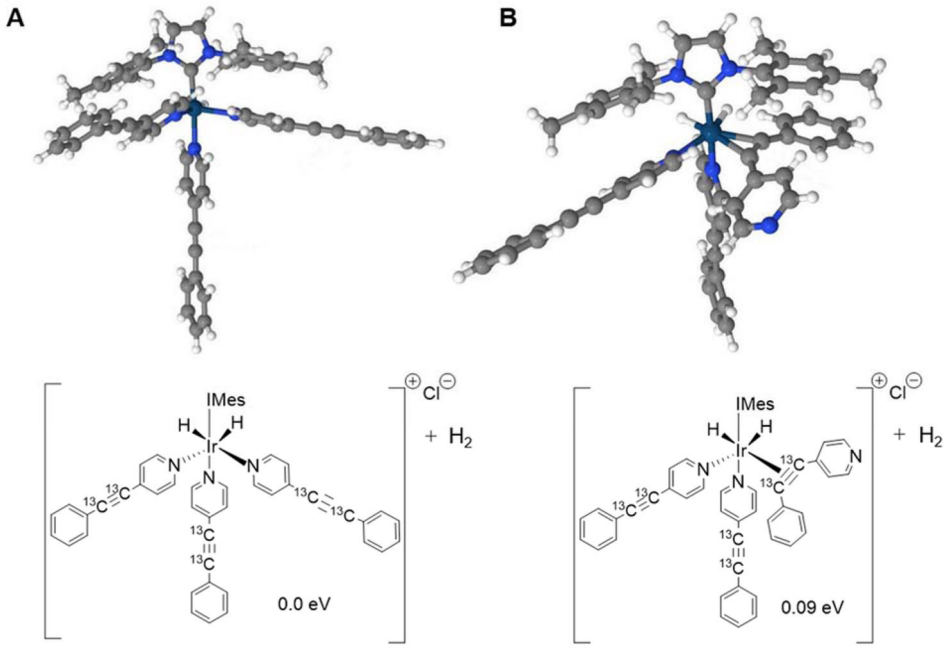

Figure 2.

Two possible polarization transfer catalysts (PTC's). Top: 3D models obtained after energy minimization in the all electron code FHI-aims. Bottom: Structural formulas of the PTCs for clarity. A) The substrate is bound to all Ir binding sites via nitrogen. B) One of the molecules' triple bond binds to the iridium catalyst, which has a higher energy than the structure in A. DFT calculations reveal that the energy difference between the two proposed complexes is relatively small (0.09 eV). Other possible complexes (with higher energies) are discussed in the SI.

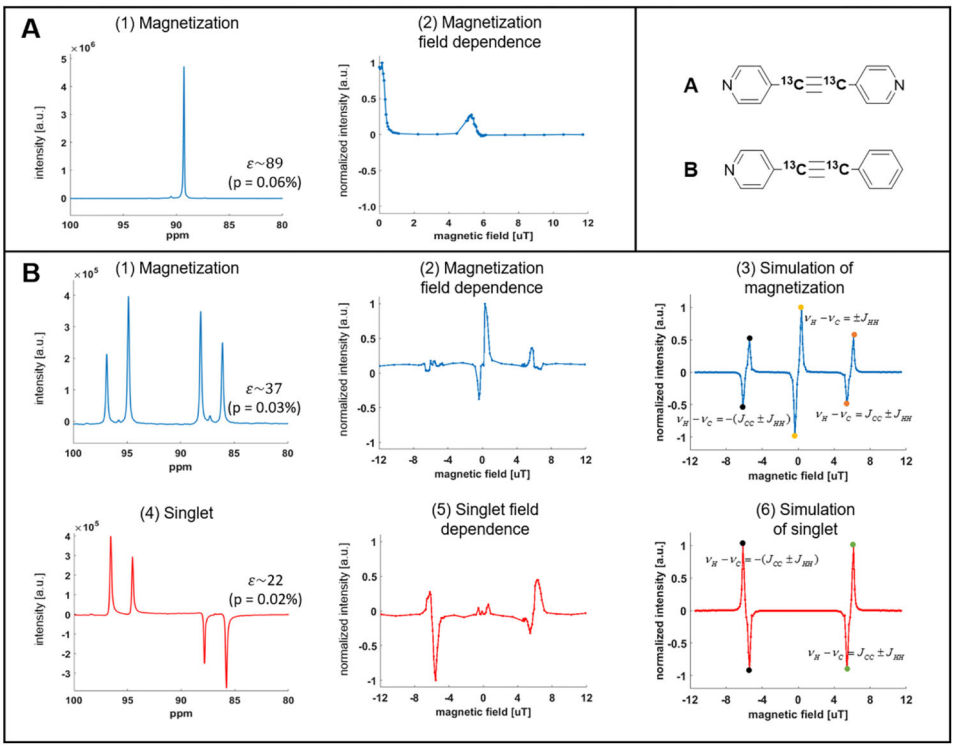

Figure 3.

Field dependent hyperpolarization for the two substrates. Panel A shows (1) a hyperpolarized magnetization spectrum hyperpolarized at 0.17 μT (and acquired at 8.45 T) for the symmetric substrate and (2) its field dependence in the μT range. Panel B shows the experimental and simulated results of creating magnetization and singlet order for the asymmetric substrate, as function of magnetic field; (1) Magnetization spectrum hyperpolarized at 0.28 μT. (2) Experimental and (3) simulated field dependence for magnetization. (4) Singlet spectrum hyperpolarized at 6.2 μT. (5) Experimental and (6) simulated field dependence for singlet order. In (B3) and (B6), the highlighted points are the local maxima for polarization transfer labeled by analytically derived resonance conditions from careful inspection of the nuclear-spin Hamiltonian provided in the SI.

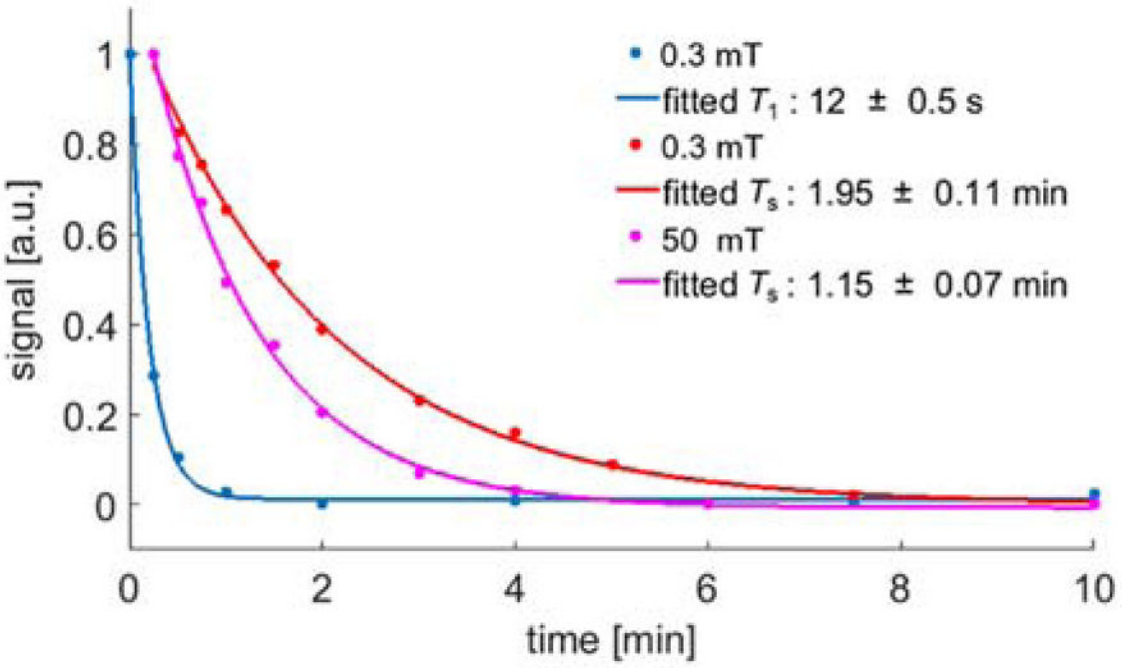

Figure 4.

T_1 and T_S measurements of 1-phenyl-2-(4-pyridyl) acetylene. For all measurements, the sample was first hyperpolarized in the shield using 0.4 μT (polarize magnetization) / 6 μT (polarize singlet order) then positioned at 0.3 mT or 50 mT. After varying delay times the sample was transferred to the magnet quickly to measure the remaining signal. The data points were sampled randomly to eliminate the effect of the slow triple bond hydrogenation, and the lifetime constants were obtained using single exponential fit.